ChemComm

Chemical Communications

www.rsc.org/chemcomm

Volume 48 | Number 51 | 28 June 2012 | Pages 6305–6436

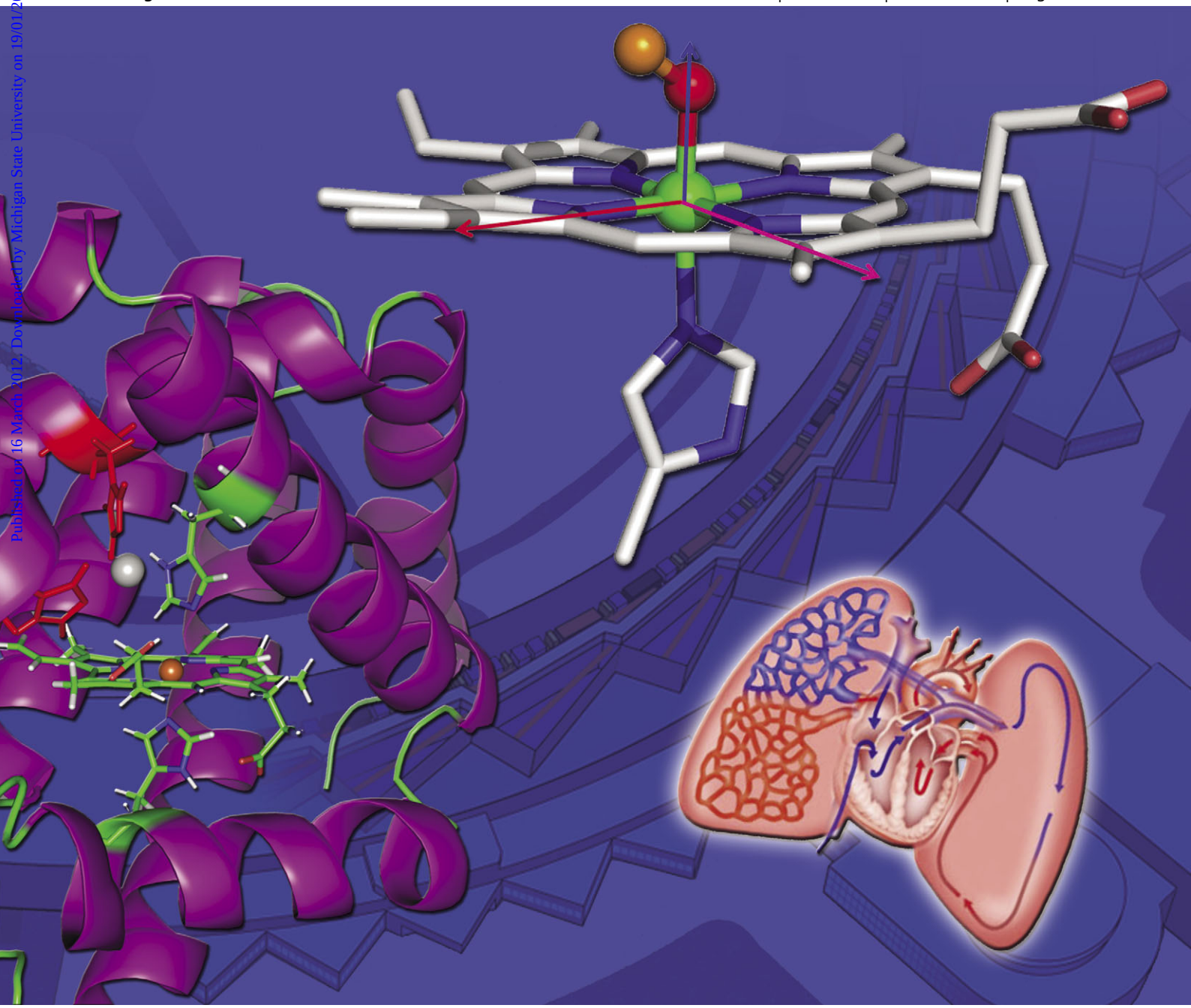

ISSN 1359-7345

RSC Publishing

COMMUNICATION

Sage *et al.*

Vibrational dynamics of oxygenated heme proteins

ChemComm

View Article Online
Dynamic Article Links

Cite this: *Chem. Commun.*, 2012, **48**, 6340–6342

www.rsc.org/chemcomm

COMMUNICATION

Vibrational dynamics of oxygenated heme proteins†‡

Weiqiao Zeng,[a] Alexander Barabanschikov,[a] Ningyan Wang,[b] Yi Lu,[b] Jiyong Zhao,[c] Wolfgang Sturhahn,[c] E. Ercan Alp[c] and J. Timothy Sage*[a]

Received 18th February 2012, Accepted 15th March 2012
DOI: 10.1039/c2cc31239e

Advanced spectroscopic techniques coupled with DFT calculations reveal the vibrational dynamics of the iron in stable dioxygen complexes with myoglobin and with a mutant engineered to model the catalytic site of heme-copper oxidases. The unprecedented level of detail will constrain computational modelling of reactions with oxygen.

Heme proteins dominate biological O_2 consumption on Earth. The reduction of molecular oxygen to water by heme-copper oxidases (HCOs) powers the metabolism of aerobic organisms,[1] and numerous heme proteins function as O_2 sensors and transporters.[2] Globins are heme proteins employed thoughout the tree of life[3] as O_2 sensors and enzymes, but are most familiar for their roles in O_2 transport and storage in vertebrate metabolism.[4] Heme-O_2 complexes (Fig. 1) hold great interest as intermediates in diverse enzymatic processes, but detection and interpretation of their vibrational properties remain challenging.

Nuclear resonance vibrational spectroscopy (NRVS; also known as nuclear inelastic scattering) provides a comprehensive and quantitative picture of the vibrational dynamics of ^{57}Fe in isotopically enriched proteins.[6] Fig. 2a and b compares vibrational densities of states (VDOS) for the heme iron atom derived from NRVS measurements on frozen solutions of O_2 complexes with the muscle pigment myoglobin (Mb) and with an L29H/F43H mutant (Cu_BMb), engineered to coordinate a second metal ion *via* histidines at positions 29, 43, and 64. With Cu(I) occupying the engineered site, Cu_BMb mimics the structure (Fig. S1, ESI‡) of HCOs, and achieves partial reduction of O_2 to produce peroxide.[7] On the other hand, substitution of the redox inert Ag(I) ion for Cu in air yields a stable Ag(I)–Cu_BMbO_2 complex,[8] which models structural and electrostatic features of the first reaction intermediate.

The Fe dynamics of the two complexes (Fig. 2) exhibit both qualitative similarities and quantitative differences. Features are

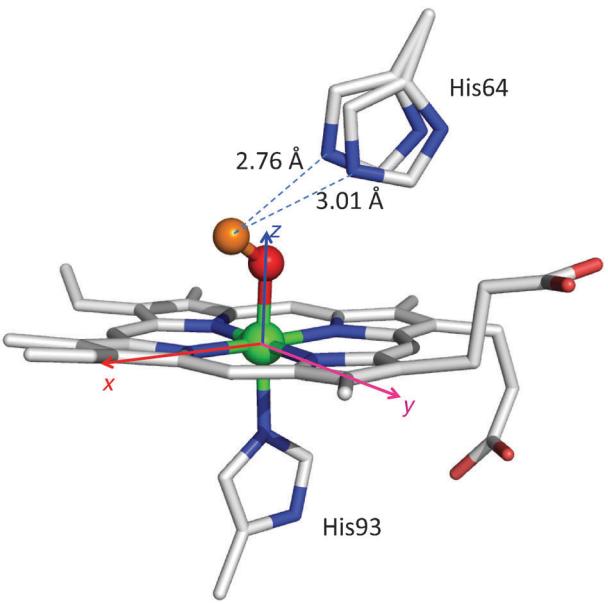

Fig. 1 Crystallographic model of the heme site of oxygenated myoglobin refined to 1.25 Å (PDB code 2Z6S),[5] with spheres highlighting the heme iron and O_2 ligand.

clearly resolved from the Ag(I)–Cu_BMbO_2 VDOS at approximately 339, 370, 428 and 588 cm^{-1}. The latter two appear at higher frequencies than corresponding features in the MbO_2 VDOS, reflecting the influence of the second metal ion on the oxygenated heme. Although we are not aware of previous applications of NRVS to oxygenated heme proteins, recent measurements on oxygenated "picket fence" porphyrins[9] identified vibrations of the FeOO fragment within 10 cm^{-1} of the 423 and 579 cm^{-1} features observed for MbO_2.

Isotopic labelling also distinguishes Fe vibrations from the dominant signal due to porphyrin vibrations in Raman scattering from frozen solutions of these molecules (Fig. 3). In particular, the 2.3 cm^{-1} upshift of the 579 cm^{-1} MbO_2 frequency when ^{54}Fe replaces ^{57}Fe is consistent with the 2 cm^{-1} shift predicted (by eqn S10) based on the 0.11 area of the 579 cm^{-1} feature in the Fe VDOS. This frequency drops to 572 cm^{-1} at ambient temperature (Fig. S2, ESI‡), where previous Raman measurements using O_2 isotopomers[10] reveal frequency shifts that we use in conjunction with the NRVS results to experimentally quantify the kinetic energy distribution (KED). More than 90% of the mode energy is localized

[a] *Department of Physics and Center for Interdisciplinary Research on Complex Systems, Northeastern University, Boston MA 02115, USA. E-mail: jtsage@neu.edu*
[b] *Department of Chemistry, University of Illinois at Urbana Champaign, Urbana IL 61801, USA*
[c] *Advanced Photon Source, Argonne National Laboratory, Argonne IL 60439, USA*

† This article is part of the *ChemComm* 'Porphyrins and phthalocyanines' web themed issue.

‡ Electronic supplementary information (ESI) available: methods, supplementary tables and figures, and animations of predicted 215, 298, 346, 373, 449, and 639 cm^{-1} vibrations. See DOI: 10.1039/c2cc31239e

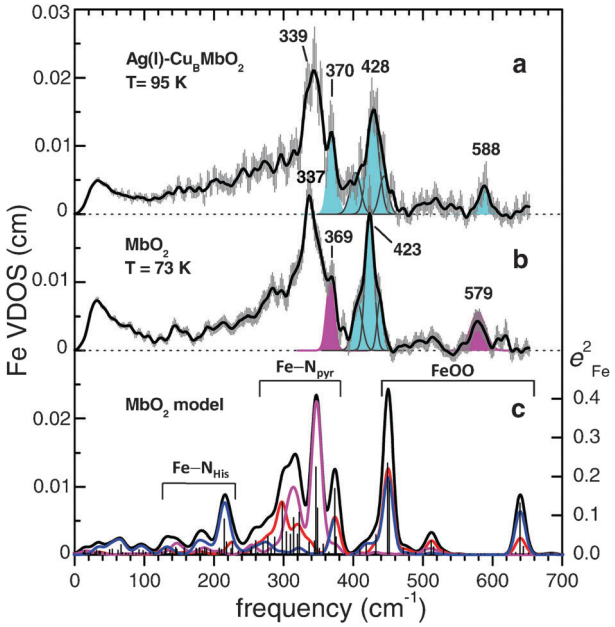

Fig. 2 The Fe VDOS determined from NRVS measurements on (a) Ag(I)–Cu$_B$MbO$_2$ and (b) MbO$_2$ completely describe vibrational motion of Fe in each molecule. Shading indicates areas determined by curve fitting the VDOS, in cyan, and estimated from ^{57}Fe/^{54}Fe isotope shifts, in magenta. The black trace in panel (c) shows the predicted Fe VDOS, indicating regions where each Fe-ligand bond contributes to the signal. Predicted contributions from motion along *x* (red), *y* (magenta), and *z* (blue) refer to the coordinate system in Fig. 1, where the four pyrrole nitrogens define the *xy* plane and the FeOO group defines the *xz* plane.

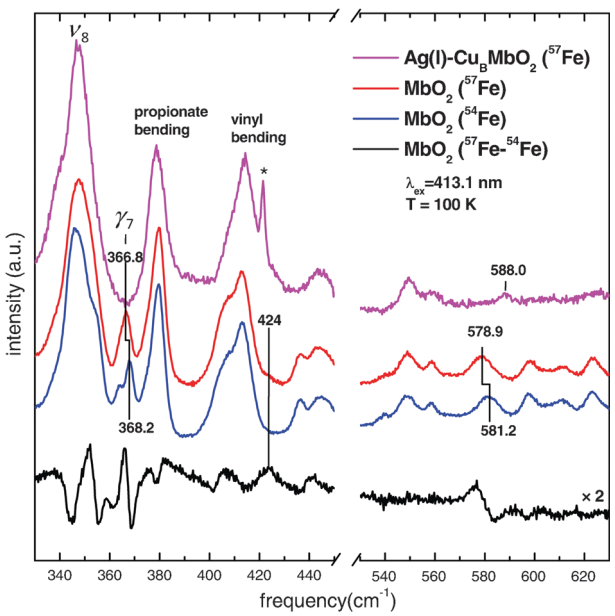

Fig. 3 Cryogenic Raman spectra recorded in resonance with the Soret absorption band include contributions from Fe vibrations, highlighted by the ^{57}Fe/^{54}Fe difference spectrum, among more strongly enhanced porphyrin vibrations.

on the FeOO fragment, with the majority (77%) on one of the oxygen atoms. The asymmetric KED is an unambiguous signature for end-on binding and distinct from the more uniform KED predicted for a two-body Fe-O$_2$ oscillator (Table 1).

Table 1 Vibrational kinetic energy distributions over the FeOO group

Protein	Frequency (cm^{-1})	e^2_{Fe}	$e^2_{O_b}$	$e^2_{O_t}$
Ag(I)–Cu$_B$MbO$_2$	428[a]	0.52[a]	—	—
Ag(I)–Cu$_B$MbO$_2$	588[a]	0.08[a]	—	—
MbO$_2$	423[a]	0.52[a]	—	—
MbO$_2$	579[a]	0.11[a]	0.77[b]	0.06[b]
MbO$_2$ model[c]	298	0.13	0.04	0.11
MbO$_2$ model[c]	449/451	0.42	0.09	0.17
MbO$_2$ model[c]	639	0.13	0.63	0.03
Fe–O$_2$ oscillator	—	0.36	0.32	0.32

[a] Determined from cryogenic NRVS measurements. [b] Determined according to eqn. S10 from isotopic frequency shifts reported at ambient temperature.[10,11] [c] DFT calculation on optimized model for the MbO$_2$ heme site (Fig. S3, ESI).

In contrast with ambient temperature Raman measurements (Fig. S2, ESI‡), improved spectral resolution at cryogenic temperatures also identifies an Fe-isotope sensitive peak at 367 cm^{-1} in MbO$_2$ that approximately corresponds in both frequency and predicted area (using eqn S10) to the 369 cm^{-1} NRVS feature, as indicated by the shaded area in Fig. 2b. Subtracting the ^{57}Fe and ^{54}Fe-enriched MbO$_2$ Raman spectra (Fig. 3) highlights the shifts of the 579 and 367 cm^{-1} bands. Additional differences in the 340–380 cm^{-1} region and near 424 cm^{-1} are difficult to quantify because they may not correspond to simple frequency shifts, although their proximity to strong NRVS signals is suggestive.

DFT calculations on a model for MbO$_2$ (Fig. S3, ESI‡) yield the VDOS for Fe (Fig. 2c), as well as for other atoms (Fig. S4 and S5, ESI‡). Significant FeOO motion contributes to a predicted 639 cm^{-1} mode (Movie S639, ESI‡), which exhibits a KED centered on the O$_b$ atom bound to the heme Fe in agreement with the observed 579 cm^{-1} mode KED (Table 1, Fig. S4, ESI‡), and an unresolved pair of modes with predicted 449 (Movie S449, ESI‡) and 451 cm^{-1} frequencies, possessing a total e^2_{Fe} = 0.42, accounting for much of the 423 cm^{-1} VDOS area. An additional predicted mode at 298 cm^{-1} (Movie S298, ESI‡) with 30% localization on FeOO does not correspond to a clearly resolved feature in the Fe VDOS.

The predicted 375 cm^{-1} vibration (Movie S375, ESI‡) corresponds closely in frequency and Fe amplitude to the band observed near 370 cm^{-1} in both NRVS and Raman. Vibrational correlation analysis[12] reveals 34% overlap with the γ_7 mode of iron porphine, which involves Fe motion perpendicular to the heme plane coupled with concurrent methine displacements, and visual examination also reveals in-plane Fe motion, coupled with rotation of the His64 imidazole ring.

Fe motion parallel to the heme plane contributes throughout the 250–400 cm^{-1} region, distinctly partitioned either parallel or perpendicular to the FeOO plane, similar in character to the vibrational anisotropy observed experimentally for single crystals of Fe nitrosyl porphyrins.[13] Specifically, comparison with the predicted VDOS implicates Fe motion perpendicular to the FeOO plane as the primary contribution to the sharp maximum in the observed signal at 337 cm^{-1}, while vibrations with significant Fe motion parallel to the FeOO plane are distributed over a wider range of frequencies.

The correspondence between predicted and observed features becomes less apparent at lower frequencies. The active site model is too small to capture global oscillations of the polypeptide that carry the heme group and account for the broad feature peaked near 30 cm^{-1}. It is conceivable that coupling with polypeptide vibrations also accounts for failure to resolve the predicted 215 cm^{-1} feature (Movie S215, ESI‡), although NRVS measurements on oxygenated picket fence porphyrins reveal a feature attributed to Fe-imidazole stretching near 200 cm^{-1}.[9]

Reproduction of the areas of prominent features above 300 cm^{-1} suggests that the MbO_2 model calculation reproduces the character of the corresponding vibrations. However, the closed-shell singlet state calculation overerestimates FeOO vibrational frequencies (Table 1), mirroring results on picket fence porphyrins, which found that spin-unrestricted DFT calculations predict an open-shell electronic configuration that significantly underestimates these frequencies.[9] Quantitative vibrational comparisons should inform the ongoing discussion of the electronic ground state of oxygenated hemes.[14]

Although 1 atmosphere of CO is not sufficient to saturate the heme site of Cu(I)–Cu_BMb,[15] Ag(I)–Cu_BMb is fully saturated with O_2 when prepared in air.[7] This suggests that O_2 affinity exceeds CO affinity by at least an order of magnitude, in contrast with native Mb, whose affinity for CO is 25 times larger than for O_2.[16] The enhanced discrimination in favor of the O_2 substrate by Ag(I)–MbO_2 is notable, since His64 ligates Ag(I) and is no longer available to hydrogen bond with O_2, as in MbO_2 (Fig. 1). Apparently, the Ag(I) ion more than compensates for the loss of the stabilizing hydrogen bond.

The increased FeOO frequencies observed for Ag(I)–$Cu_B$$MbO_2$ in comparison with MbO_2 are consistent with a strengthened Fe-O_2 bond. The Fe centered 428 cm^{-1} FeOO vibration of Ag(I)–$Cu_B$$MbO_2$ presumably corresponds to the 435 cm^{-1} frequency reported in the transiently formed O_2 complex with cytochrome *c* oxidase,[10] and both FeOO frequencies lie at the upper end of the range reported for oxygenated heme proteins (Table S1, ESI‡). Thus, Cu_BMb reproduces vibrational as well as functional HCO properties. Protein engineering yields a stable O_2 complex that mimics the first intermediate in the reaction of fully reduced HCO with O_2, and its vibrational behavior should guide the course of computational investigations.

We acknowledge financial support from the National Science Foundation (CHE-1026369) and the National Institutes of Health (GM-062211), and thank I. Petrik for helpful comments. Use of the Advanced Photon Source was supported by the U.S. Department of Energy, Basic Energy Sciences, Office of Science, under Contract No. DEAC02-06CH11357.

References

1 P. Brzezinski and R. B. Gennis, *J. Bioenerg. Biomembr.*, 2008, **40**, 521–531.
2 K. R. Rodgers, *Curr. Opin. Chem. Biol.*, 1999, **3**, 158–167.
3 S. N. Vinogradov and L. Moens, *J. Biol. Chem.*, 2008, **283**, 8773–8777.
4 J. B. Wittenberg, *Gene*, 2007, **398**, 156–161.
5 M. Unno, H. Chen, S. Kusama, S. Shaik and M. Ikeda-Saito, *J. Am. Chem. Soc.*, 2007, **129**, 13394–13395.
6 (*a*) W. Zeng, N. J. Silvernail, W. R. Scheidt and J. T. Sage, *in Nuclear Resonance Vibrational Spectroscopy (NRVS)*, John Wiley & Sons, Ltd., Chichester, UK, 2007, pp. 401–421; (*b*) W. Sturhahn, *J. Phys.: Condens. Matter*, 2004, **16**, S497–S530.
7 J. A. Sigman, H. K. Kim, X. Zhao, J. R. Carey and Y. Lu, *Proc. Natl. Acad. Sci. U. S. A.*, 2003, **100**, 3629–3634.
8 J. A. Sigman, B. C. Kwok and Y. Lu, *J. Am. Chem. Soc.*, 2000, **122**, 8192–8196.
9 J. Li, Q. Peng, A. Barabanschikov, J. W. Pavlik, E. E. Alp, W. Sturhahn, J. Zhao, C. E. Schulz, J. T. Sage and W. R. Scheidt, *Chem.–Eur. J.*, 2011, **17**, 11178–11185.
10 (*a*) S. Hirota, T. Ogura, E. H. Appelman, K. Shinzawah-Itoh, S. Yoshikawa and T. Kitagawa, *J. Am. Chem. Soc.*, 1994, **116**, 10564–10570; (*b*) S. Jeyarajah, L. M. Proniewicz, H. Bronder and J. R. Kincaid, *J. Biol. Chem.*, 1994, **269**, 31047–31050.
11 T. Tomita, S. Hirota, T. Ogura, J. S. Olson and T. Kitagawa, *J. Phys. Chem. B*, 1999, **103**, 7044–7054.
12 A. Barabanschikov, A. Demidov, M. Kubo, P. M. Champion, J. T. Sage, J. Zhao, W. Sturhahn and E. E. Alp, *J. Chem. Phys.*, 2011, **135**, 015101.
13 J. W. Pavlik, A. Barabanschikov, A. G. Oliver, E. E. Alp, W. Sturhahn, J. Zhao, J. T. Sage and W. R. Scheidt, *Angew. Chem., Int. Ed.*, 2010, **49**, 4400–4404.
14 H. Chen, M. Ikeda-Saito and S. Shaik, *J. Am. Chem. Soc.*, 2008, **130**, 14778–14790.
15 C. Lu, X. Zhao, Y. Lu, D. L. Rousseau and S.-R. Yeh, *J. Am. Chem. Soc.*, 2010, **132**, 1598–1605.
16 M. L. Quillin, T. Li, J. S. Olson, G. N. Phillips, Y. Dou, M. Ikeda-Saito, R. Regan, M. Carlson, Q. H. Gibson and H. Li, *J. Mol. Biol.*, 1995, **245**, 416–436.

